Scripta Materialia 119 (2016) 71–75

Contents lists available at ScienceDirect

Scripta Materialia

journal homepage: www.elsevier.com/locate/scriptamat

Regular Article

A direct comparison between in-situ transmission electron microscopy observations and Dislocation Dynamics simulations of interaction between dislocation and irradiation induced loop in a zirconium alloy

J. Drouet [a,b], L. Dupuy [a,*], F. Onimus [a], F. Mompiou [b]

[a] DEN-Service de Recherches Métallurgiques Appliquées, CEA, Université Paris-Saclay, F-91191 Gif-sur-Yvette, France
[b] CEMES-CNRS and Université de Toulouse, 29, rue J. Marvig, 31055 Toulouse, France

ARTICLE INFO

Article history:
Received 14 January 2016
Received in revised form 28 March 2016
Accepted 29 March 2016
Available online xxxx

Keywords:
In situ transmission electron microscopy
Dislocation Dynamics
Zirconium alloy

ABSTRACT

Dislocation Dynamics simulations of a dislocation-loop interaction are compared to experimental observations performed during an in-situ straining experiment in a Transmission Electron Microscope at 500 °C on a zirconium alloy, referred to as recrystallized Zircaloy-4, irradiated with Zr ions. The DD simulations, performed in the same geometrical, stress and dislocation mobility conditions, exhibit an excellent agreement with the observed interaction. It is shown that the interaction leads to the formation of an helicoidal turn expanding along the dislocation before being blocked below the sample surface. This approach opens the way to massive Dislocation Dynamics simulations with realistic input data.

Zirconium alloys are used in the nuclear industry as fuel rod cladding tube of Pressurized Water Reactor fuel assemblies. The fast neutron irradiation, undergone by the material, alters its microstructure, thus modifying its mechanical behavior. Indeed, previous studies have shown that neutron irradiation induces a high density of small prismatic loops, with $\langle a \rangle$ Burgers vectors, lying in the prismatic planes [1–3]. During post-irradiation mechanical tests, these loops are cleared, or swept out, by gliding dislocations creating, inside the grain, a thin zone free of defects where further dislocations can easily glide [4,5]. Detailed observations have proven that, in this case, slip occurs preferably in the basal plane, a puzzling fact as dislocations mainly glide in the prismatic plane in unirradiated conditions. This change of preferential slip system has been attributed to different reactions between loop and dislocation depending on whether the latter glides in the prismatic or basal planes [4,6,7]. Thus a thorough understanding of the effect of irradiation requires a good characterization of elementary interactions between dislocations and loops.

In that perspective, in-situ transmission electron microscopy (TEM) experiments on ion irradiated samples appear to be well adapted to probe real time dislocation interactions as shown in [7]. On the modeling side, Dislocation Dynamics (DD) [8] and Molecular Dynamics (MD) [9] simulations have also been undertaken in the case of Zr. While in-situ TEM observations provide valuable information on the occurrence of such interactions and their dynamics in the real material, they fail in retrieving the details of the interactions at the loop scale (<20 nm). On the contrary, DD simulations are able to describe accurately the interactions at such scale, but inputs such as the dislocation mobility law and appropriate stress level are needed. In order to bridge experiments and simulations, we have quantitatively compared the interaction of a dislocation gliding in a pyramidal plane at 500 °C with a loop, observed during an in-situ TEM test, with a DD simulation performed in the same geometrical configuration, time scale and stress conditions. The detailed comparison between simulation and experiment validates our understanding of this interaction mechanism and gives credit to our multi-scale approach.

1. Experimental

Recrystallized Zy-4 tensile test specimens, have been irradiated on a specifically designed holder with 600 keV Zr ions at 340 °C [10] up to a dose of 8×10^{17} ions/m^2 at the ARAMIS facility (CSNSM/IN2P3/CNRS, Orsay). The irradiation damage profile obtained by TRIM calculations [11], increases from the surface up to a peak located at about 120 nm from the outer surface and decreases progressively down to 350 nm deep. Before irradiation the samples were electropolished on one side. After irradiation the irradiated surface was protected by a varnish and the rear surface was eventually electropolished to create an electron transparent area <200 nm thick, i.e. fully irradiated by Zr ions. In these conditions the microstructure consists of small dislocation loops with $\langle a \rangle$ Burgers vectors with a mean diameter of 15 nm and number density of 1.2×10^{21} m^{-3}. Furthermore 92% of the largest loops analyzed were of vacancy nature. The tensile test sample is then positioned on a

* Corresponding author.
E-mail addresses: julie.drouet@cea.fr (J. Drouet), laurent.dupuy@cea.fr (L. Dupuy), fabien.onimus@cea.fr (F. Onimus), mompiou@cemes.fr (F. Mompiou).

http://dx.doi.org/10.1016/j.scriptamat.2016.03.029
1359-6462/

custom-made straining and heating TEM sample holder [12]. The experiments were carried out in a JEOL 2010HC operating at 200 kV. Video sequences are recorded using a MEGAVIEW III camera and a DVD recorder. Electron diffraction was used to determine the grain orientation. The temperature of the specimen is increased up to a temperature between 450 °C to 500 °C. At the required temperature the sample is deformed in situ by imposing a series of strain increments. Among all the interactions observed, one of the clearest has been chosen for the present purpose to undertake both a detailed analysis and DD simulations. DD simulations were performed using the nodal code NUMODIS [8]. Dislocation lines are discretized into a series of interconnected linear segments characterized by a Burgers vector and a glide plane. Linear mobility laws were chosen for dislocation glide in prismatic, pyramidal-⟨a⟩ and basal planes. No dislocation climb or cross-slip was explicitly taken into account in the present study. The junction reactions are selected based on the maximum-dissipation principle [13] and special care was given to consider all crystallographically possible outcomes.

2. Results

2.1. Data extracted from the experiment and introduced into the numerical simulation

The observed interaction is shown on Fig. 3 by a series of bright field (BF) images extracted from the video sequence and taken under the diffraction vector $\vec{g} = (10\bar{1}1)$. The investigated interaction took place between a dislocation gliding in a pyramidal plane $(01\bar{1}1)$ with a Burgers vector assumed to be of ⟨a⟩ type, namely $\vec{b}_d = 1/3[\bar{2}110]$. Indeed, ⟨c + a⟩ first order pyramidal slip is known to be a very hard slip system and is observed only when straining along the ⟨c⟩ direction. The observation of ⟨a⟩-pyramidal slip can be attributed to the high test temperature. Indeed this system has frequently been observed during cross-slip in similar conditions [14,15]. The observation of partially cleared pyramidal channels during tensile test at high temperature after neutron irradiation also indicates the activation of this slip system [4,16]. The 3D geometrical configuration, which corresponds to a crystal orientation with $x = [\bar{1}2210\bar{6}]$, $y = [8\bar{1}683]$ and $z = [5\bar{2}712]$, is shown schematically in Fig. 1a. The 2D projection along the electron beam direction z is shown with the BF image in Fig. 1c. The trace of the glide plane (*tr.*) with the surface is also marked. It is almost parallel to the long segments of the dislocation indicating that these segments are stuck beneath the surface, presumably by an oxide layer. A small hexagonal prism is shown to indicate schematically the axes and gliding plane. Before straining along the axis *T*, the dislocation is pinned by a small precipitate noted *P* in Fig. 1. The thickness of the sample, 162 nm, was deduced from the distance between the slip traces and from the knowledge of the orientation of the gliding plane. Based on this experimental information, a DD simulation was set up in order to compute the interaction between the dislocation and the loop and compare it with the experiment. The size of the simulation box chosen is 1200 nm along the *x*-direction, 360 nm along the *y*-direction, 162 nm along the *z*-direction. The two surfaces, at the top and bottom of the box, are treated as two dislocation impenetrable surfaces. A dislocation is introduced as a 500 nm long Frank-Read source of screw character in the pyramidal plane $(01\bar{1}0)$ with a Burgers vector $1/3[\bar{2}110]$. A dislocation loop (l) is set in front of the moving dislocation. Its size of about 19 nm is deduced from TEM observations. Its habit plane and Burgers vector are however difficult to determine experimentally beforehand. All the second order prismatic planes were therefore tested systematically in DD simulations to determine a posteriori its habit plane. In the following, we show the results obtained with a loop in the $(\bar{2}110)$ plane. Similarly, the exact position of the dislocation loop is not known in the *z* direction. Several positions were considered over a certain distance range Δh as shown schematically in Fig. 1b. Finally, the choice of a vacancy loop was made in order to obtain a better agreement between simulation and experiment considering the shape of the dislocation after the interaction.

The drag coefficient B is an important parameter that can be tentatively measured experimentally. This can be done by measuring the variation of the dislocation speed with respect to the stress as explained below [14]. When the dislocation is immobile, the applied resolved shear stress (τ) counterbalances the line tension stress (τ_l) (Fig. 2a). The origin of the viscosity is related to the existence of a friction force (τ_f) that is opposed to the motion (Fig. 2b), and which can be taken as $\tau_f = Bv/b$. When the dislocation moves at a given speed v, the equilibrium condition is modified to $\tau = \tau_l + \tau_f$ (Fig. 2b). If we assume that the applied stress is constant during a short period of time ($\Delta\tau = 0$) where the dislocation is observed, the variation of the line tension stress $\Delta\tau_l$ is then equal to $B\Delta v/b$. Two measures of the dislocation speed with respect to the line tension stress have been performed. Fig. 2c and d shows two image differences taken during a time interval of 2 s. The geometrical perspective effects due to the glide plane inclination have been corrected. The initial position of the dislocation appears in black while the final position is in white. This allows the measurement of the distance traveled and thus the speed. The equilibrium shapes of the dislocation in Fig. 2c and d can be fitted on a theoretical shape calculated by anisotropic elasticity using the DISDI software [17] (Fig. 2e), allowing the determination of the line tension stress. This leads to $\tau_l = 40$ MPa for $v = 11$ nm/s (Fig. 2c) and $\tau_l = 44$ MPa for $v = 6.5$ nm/s and thus to $B = b\Delta\tau/\Delta v = 0.3$ MPa · s. The uncertainty on the speed, i.e. ± 1 nm/s and on the stress ± 2 MPa leads to $0 < B \leq 1.1$ MPa·s. The applied stress can be estimated by extrapolating the value of the line tension for $v = 0$, leading to $\tau = 50$ MPa for $B = 0.3$ MPa·s ($38 < \tau < 80$ MPa considering uncertainty in *B*.). For the DD simulations, we then took $B = 0.3$ MPa·s for pyramidal and prismatic slip systems. A value of 3 MPa·s has been chosen for the basal slip in order to account for the difficult activation of this slip system. Indeed, this slip system has never been observed in

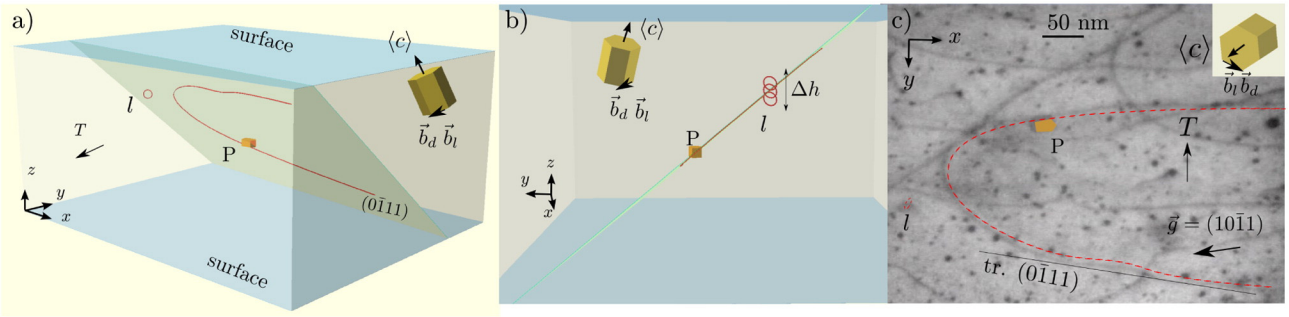

Fig. 1. a) Schematic view of the geometry of the dislocation loop interaction. b) shows different possible positions of the loop (l) in the *z* direction when the glide plane is seen edge-on. c) is the TEM image superimposed with the projected configuration in the *xy* plane. *T* is the straining direction, *P* a precipitate. *tr* indicates the intersection of the glide plane with the surface. The dislocation and loop Burgers vectors are indicated on the hexagonal prism.

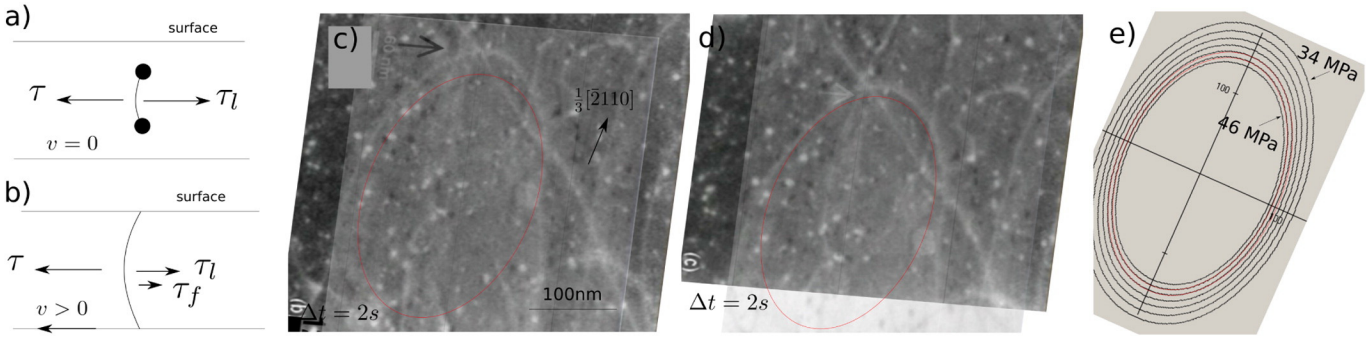

Fig. 2. Stress equilibrium conditions for an immobile a) or a moving b) dislocation. c) and d) are image differences ($\Delta t = 2$ s) allowing both dislocation speed and line tension stress measurements using anisotropic elastic calculations (e).

our experiments. Knowing the Schmid factor for the slip system, $s_f = 0.31$, the applied stress was taken as $\sigma = \tau/s_f = 160$ MPa. These high drag coefficients lead us to select an appropriate time-step of 4 ms, which is in turn higher than time-steps usually used in DD simulations.

2.2. Results of the DD simulation and comparison with experimental observations

During the time preceding the interaction (Fig. 3a), the dislocation glides first toward the loop, the dislocation segment close to the loop being temporarily stopped in the vicinity of the loop during 6.1 s. Eventually the interaction occurs (Fig. 3b). After the loop incorporation (Fig. 3c), the dislocation becomes more and more wavy (Fig. 3d), indicating the presence of an helix turn expanding along the dislocation line. This same configuration has been simulated by DD. Simulations were performed with the three possible Burgers vectors for the loop, and lead to the creation of an helix turn on the dislocation. Vacancy or interstitial loops have also been investigated systematically, as in a previous study [8].

The best configuration, which fits the most adequately the experiment, and especially the wavy shape of the dislocation after the interaction, has been obtained with a vacancy loop that has the same Burgers vector as the gliding dislocation. The result of this simulation performed with a square vacancy loop, of 19 nm side, with a Burgers vector $\vec{b}_l = 1/3[\bar{2}110]$ and a dislocation with a Burgers vector $\vec{b}_d = 1/3[\bar{2}110]$ gliding in the pyramidal plane $(01\bar{1}1)$ is compared with the interaction observed in situ by TEM on Fig. 3. For comparison, the same time scale in the simulation and in the experiment was used (see the video in the supplementary materials). The initial time step has been chosen so that the contact between the dislocation and the loop occurs at the same time (here $t = 0$ s, Fig. 3b). It can be noted that the simulation reproduces well the glide of the dislocation toward the loop (see also the movie in the supplemental materials). When the interaction occurs it can be seen in the simulation that the loop is incorporated as an helix turn into the dislocation. This helix turn then expands along the dislocation (from $t = 0$ s to $t = 7.8$ s).

3. Discussion

The Dislocation Dynamics simulation with the appropriate ingredients accurately reproduces the kinetics of the interaction as well as the shape and curvature of the dislocation all along the glide motion. The small discrepancies can be attributed in a first place to an incomplete description of the exact microstructure, especially the presence of a precipitate that has pinned the dislocation. Image forces due to the sample surfaces, were not considered in DD simulations, and may also slightly affect the shape of the dislocation. Indeed, the image force can be considered negligible in first approximation if $\sigma_i = \mu b/4\pi d$, where d is the distance to the surface, is less than the line tension stress $\sigma_l = \mu b/4\pi R$, where R is the curvature radius of the dislocation ($R = 102$ nm for screw and $R = 68$ nm for edge segments), i.e. if $d > R$. This condition is obviously not fulfilled for the screw segments as they approach the surface (see Fig. 1). Considering that the glide plane is about 250 nm large, the edge segments, which interact with the loop, and located close to the middle of the plane are sufficiently far from the surfaces. The image forces can thus be neglected when considering only the edge segments in the middle of the plane. Another interesting feature deduced from this experiment concerns the friction coefficient (B). Indeed the value of the friction coefficient measured is <1.1 MPa·s. These values are in agreement with recent measurements in a non-irradiated recrystallized Zr alloy [14]. Furthermore, considering a typical mobile dislocation density of 10^{12} m^{-2} for recrystallized zirconium alloys, the Orowan equation, $\dot{\epsilon} = \rho b^2 \sigma/B$, applied to the bulk material with the same applied shear stress leads to a strain rate between 2.3×10^{-5} s^{-1} to 1.8×10^{-4} s^{-1} which are reasonable values in these loading conditions. However, the friction coefficient (B) measured in these experiments is much higher than the value usually deduced from MD simulations. Indeed, several authors [9,18] have obtained values for the friction coefficient going from 2×10^{-5} to 10^{-4} Pa·s. which is ten orders of magnitude lower than the experimental value. This huge discrepancy may be attributed to the fact that the material studied here is not a pure metal. Alloying elements, and especially oxygen atoms [19–21], strongly affect the dislocation glide mobility. Contrary to MD simulation where the friction stress is due to phonon drag, the friction force in an industrial Zr alloy can be due to other mechanisms. At the temperature where the interaction was observed, the dislocation mobility is supposed to be controlled by the diffusion of atomic impurities as indicated by an important dynamic strain aging. According to Friedel [22], the velocity of a dislocation controlled by mobile impurities is given by $v = Db^2\tau/kT$, i.e. $B = kT/Db$, where D is the diffusion coefficient of the impurities. Considering that the impurities are oxygen atoms, the diffusion coefficient at temperature T can be expressed as $D = 6.61 \times 10^{-6} \exp(-1.91 eV/kT)$ [23]. Taking $T = 500$ °C and, $b = 0.108$ nm leads to $B = 42$ MPa·s. Although a smaller experimental value is found in this work, which can be due to a higher diffusion coefficient in the dislocation core, this calculation indicates that high friction coefficient in impure materials can be thus expected.

The very good agreement obtained between Dislocation Dynamics simulations and in situ straining experiments validates our understanding of the interaction between loops and dislocations gliding in the pyramidal plane with $\langle a \rangle$ Burgers vectors. A similar agreement can therefore be expected for the interactions between loops and dislocations gliding in prismatic planes, as dislocation interactions maps given by [24] are very similar for prismatic and pyramidal planes. The impact of the observed mechanism on the plastic behavior is not yet fully understood. Based on the mechanism described in a numerical study on irradiated FCC metal [25], while the motion of screw segments is

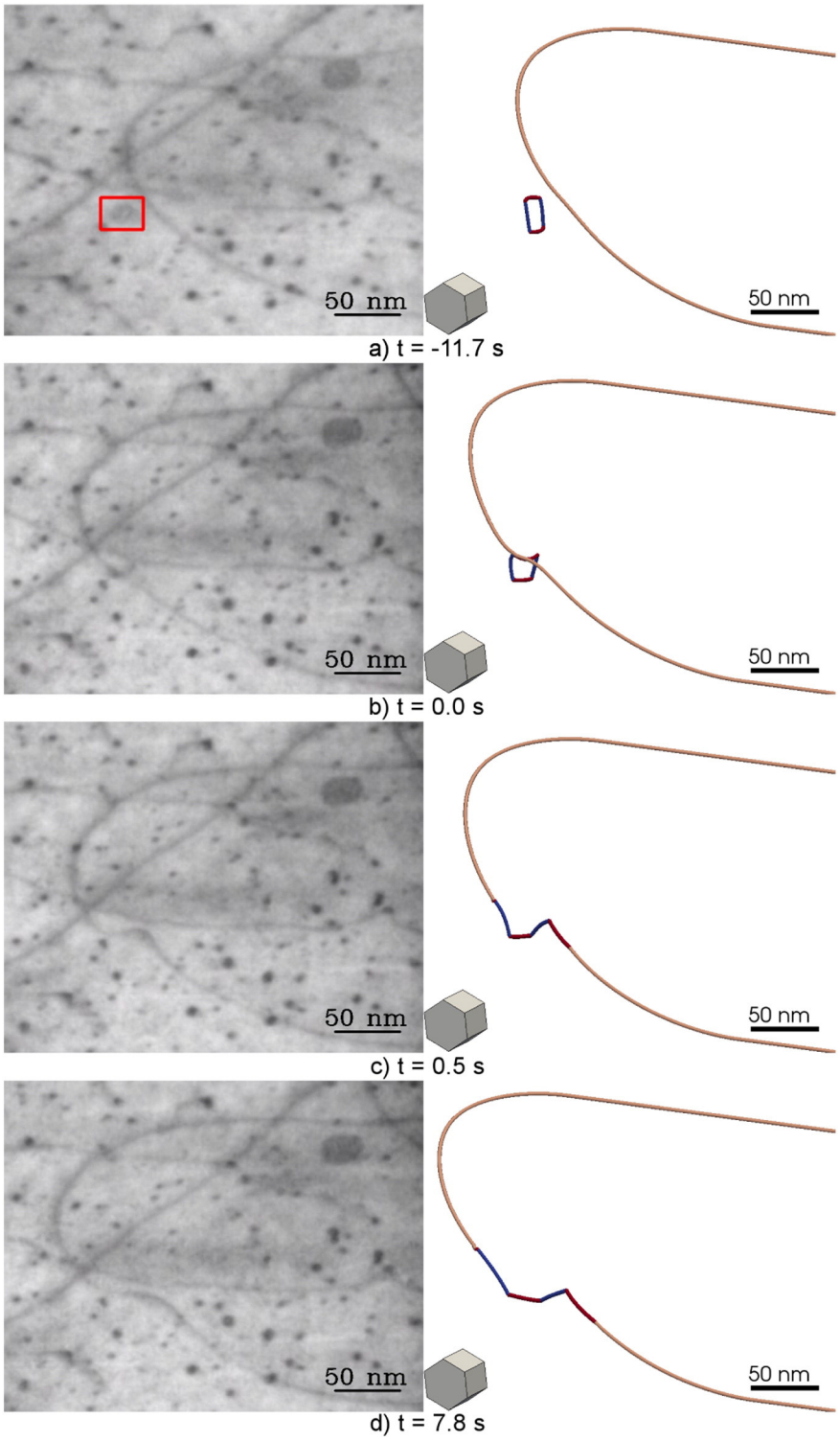

Fig. 3. Direct comparison between DD simulation and TEM observation of the dislocation loop interaction. Time reference is set to zero at the dislocation loop contact.

impeded by helicoidal turns resulting from dislocation-loop interactions, the edge parts can expand, pushing the helicoidal turns on the sides. Limited softening by edge dislocation segments is therefore expected, but some hardening should remain due to the locking of the screw parts. Based on an earlier study [8], this analysis should apply to prismatic and pyramidal glide. However, concerning basal slip, the loops or helical turns can always be pushed away along their glide cylinder leading to significant softening and dislocation channeling.

Further works are still in progress concerning a detailed comparison between MD simulations performed by Serra and Bacon [9] and DD simulations. On the experimental side, the evaluation of the friction coefficient in the other glide planes appears of fundamental importance to describe adequately the dynamics. In the long term, this study opens the way to large scale Dislocation Dynamics simulations in order to investigate the dislocation channeling mechanisms and get a better understanding and prediction of the effects of irradiation on zirconium alloys.

Acknowledgments

The authors are grateful to EDF, AREVA, and ANR ("Investissement d'Avenir" ANR-10-EQPX-38-01 for in-situ TEM and ANR-10-COSI-0011 for DD simulations) for the financial support. The authors acknowledge M. Blétry, M. Fivel, E. Ferrié, A. Etcheverry and O. Coulaud for NUMODIS development, and D. Caillard for fruitful discussions.

Appendix A. Supplementary data

Supplementary data to this article can be found online at http://dx.doi.org/10.1016/j.scriptamat.2016.03.029.

References

[1] D.O. Northwood, R.W. Gilbert, L.E. Bahen, P.M. Kelly, R.G. Blake, A. Jostsons, R.B. Adamson, J. Nucl. Mater. 79 (1979) 379–394.
[2] M. Griffiths, J. Nucl. Mater. 159 (1988) 190–218.
[3] F. Onimus, J. Béchade, Comprehensive Nuclear Materials, vol. 4, Elsevier, 2012.
[4] F. Onimus, I. Monnet, J. Béchade, C. Prioul, P. Pilvin, J. Nucl. Mater. 328 (2004) 165–179.
[5] F. Onimus, J. Béchade, D. Gilbon, Metall. Mater. Trans. A 44 (2013) 45–60.
[6] C. Régnard, B. Verhaeghe, F. Lefebvre-Joud, C. Lemaignan, in: 13th International Symposium ASTM STP vol. 1423 (2002) 384.
[7] F. Onimus, L. Dupuy, F. Mompiou, Prog. Nucl. Energy 57 (2012) 77–85 (Nuclear Materials: Selected articles from the E-MRS 2011 Spring Meeting).
[8] J. Drouet, L. Dupuy, F. Onimus, F. Mompiou, S. Perusin, A. Ambard, J. Nucl. Mater. 449 (2014) 252–262.
[9] A. Serra, D.J. Bacon, Model. Simul. Mater. Sci. Eng. 21 (2013) 045007.
[10] H. Bernas, J. Chaumont, E. Cottereau, R. Meunier, A. Traverse, C. Clerc, M. Salom, Nucl. Inst. Methods Phys. Res. B 62 (1992) 416–420.
[11] J.F. Ziegler, M.D. Ziegler, J.P. Biersack, Nucl. Inst. Methods Phys. Res. B 268 (2010) 1818–1823.
[12] A. Rajabzadeh, M. Legros, N. Combe, F. Mompiou, D.A. Molodov, Philos. Mag. 93 (2013) 1299–1316.
[13] V. Bulatov, W. Cai, Computer Simulations of Dislocations, vol. 3, Oxford University Press, 2006.
[14] D. Caillard, M. Rautenberg, X. Feaugas, Acta Mater. 87 (2015) 283–292.
[15] M. Rautenberg, X. Feaugas, D. Poquillon, J.-M. Cloué, Acta Mater. 60 (2012) 4319–4327.
[16] F. Onimus, J.L. Béchade, C. Prioul, P. Pilvin, I. Monnet, S. Doriot, B. Verhaeghe, D. Gilbon, L. Robert, L. Legras, et al., in: Zirconium in the Nuclear Industry: Fourteenth International Symposium, ASTM International, 2005.
[17] J. Douin, P. Veyssière, P. Beauchamp, Philos. Mag. 54 (1986) 375–393.
[18] L. Kubin, Dislocations, Mesoscale Simulations and Plastic Flow, vol. 5, Oxford University Press, 2013.
[19] J. Derep, S. Ibrahim, R. Rouby, G. Fantozzi, Acta Metall. 28 (1980) 607–619.
[20] D. Caillard, J. Martin, Thermally Activated Mechanisms in Crystal Plasticity, vol. 1, Pergamon, Cambridge, 2003.
[21] E. Clouet, Phys. Rev. B 86 (2012) 144104.
[22] J. Friedel, Dislocations, Pergamon Press, Oxford, 1964.
[23] I.G. Ritchie, A. Atrens, J. Nucl. Mater. 67 (1977) 254–264.
[24] B. Devincre, Philos. Mag. 93 (2013) 235–246.
[25] T. Nogaret, D. Rodney, M. Fivel, C. Robertson, J. Nucl. Mater. 380 (2008) 22–29.